water

MDPI

Article

Estimation of Evapotranspiration in the Desert–Oasis Transition Zone Using the Water Balance Method and Groundwater Level Fluctuation Method—Taking the *Haloxylon ammodendron* Forest at the Edge of the Gurbantunggut Desert as an Example

Ping Jiao [1,2,3] and Shun-Jun Hu [1,3,*]

[1] State Key Laboratory of Desert and Oasis Ecology, Xinjiang Institute of Ecology and Geography, Chinese Academy of Sciences, Urumqi 830000, China
[2] School of Resources and Environment, University of Chinese Academy of Sciences, Beijing 100000, China
[3] National Field Scientific Observation and Research Station of Akesu Oasis Farmland Ecosystem, Aksu 843000, China
* Correspondence: xjhushunjun@aliyun.com; Tel.: +86-135-7997-6452

Abstract: Shallow groundwater is an important water source for *Haloxylon ammodendron* (*H. ammodendron*). The accurate estimation of evapotranspiration (ET_g) from groundwater is of great significance for the water cycle and the maintenance of ecological stability. Using a combination of the water balance method and the groundwater level fluctuation method (*WTF*), the water balance components (precipitation, soil moisture, groundwater depth, and Bowen ratio meteorological data) in the desert–oasis transition zone were continuously monitored from 2015 to 2018 and the ET_g was estimated The results showed that the closed degree of Bowen specific energy after data screening was higher, and the annual actual evapotranspiration (ET_a) value could be reliably calculated at 260.87 mm. As the main contributor to water consumption in the growing season, latent heat accounted for 70.16~91.86% of the energy balance. Precipitation had no significant impact on water consumption for *H. ammodendron* vegetation growth, and the precipitation in the main growing season accounted for 59.44% of the ET_a. The groundwater depth in the study area decreased yearly and had a significant impact on the growth of *H. ammodendron* vegetation. Although the groundwater depth in the study area was greater than 9 m, the ET_g, as an important part of the water balance, was found to participate in the evapotranspiration process brought about by *H. ammodendron* due to the strong root system and supporting capillary water in the soil. The actual evapotranspiration ET_a for *H. ammodendron* in the main growing season was 244.32 mm, and the contribution rate for ET_g was as high as 74.78% or approximately 182.35 mm. After the ET_g was verified using the water balance method and *WTF*, *R* was greater than 0.96, the *RMSE* range was 1.5931~4.5706, the bias range was −0.15~0.11, and the *IOA* value was greater than 0.95. The accuracy of the estimation model was high, and the results were relatively accurate. The model can be applied in the desert–oasis transition zone to obtain accurate ET_g estimations and provide theoretical guidance and a scientific basis for local water resource management and ecological protection.

Keywords: shallow groundwater; water balance method; groundwater level fluctuation method; *Haloxylon ammodendron* bush; groundwater evapotranspiration

Citation: Jiao, P.; Hu, S.-J. Estimation of Evapotranspiration in the Desert–Oasis Transition Zone Using the Water Balance Method and Groundwater Level Fluctuation Method—Taking the *Haloxylon ammodendron* Forest at the Edge of the Gurbantunggut Desert as an Example. *Water* **2023**, *15*, 1210. https://doi.org/10.3390/w15061210

Academic Editor: Aizhong Ye

Received: 17 February 2023
Revised: 13 March 2023
Accepted: 16 March 2023
Published: 20 March 2023

1. Introduction

The fifth report of the IPCC pointed out that the global temperature has risen by 0.85 °C in the past 130 years. Against the background of global warming, drought, and desertification have become increasingly serious. Since the 1990s, in particular, the intensification of global warming has seriously affected all aspects of production and life in human societies [1,2]. As in other regions in the world, persistent high-temperature events have

increased significantly in most regions of China, with the most serious in the northwest. The current challenge is determining how to effectively manage water resources and accurately assess climate events [3]. On the one hand, global warming is leading to the acceleration of the water cycle and the increase in surface evaporation is leading to a decrease in the effective available water, resulting in the intensification of extreme drought events and desertification. On the other hand, as the temperature rises, the water holding capacity of the atmosphere is increasing, which means that more water vapour is needed to saturate the air and form effective precipitation [4,5]. In this context, it is of great significance for local water resource allocation and scientific management to consider the evapotranspiration from groundwater brought about by *Haloxylon ammodendron* (*H. ammodendron*) in the desert–oasis transition zones.

The desert–oasis transition zone refers to the ecological ecotone between the oasis ecosystem and the desert ecosystem, and it is a region that is very sensitive to climate change [6–9]. Such zones demonstrate a plant gradient phenomenon generated by an environmental gradient with water as the leading factor, and they are ecologically fragile zones with a sensitive degradation trend. The desert–oasis transition zone at the edge of the Gurbantunggut Desert is home to approximately 68% of the *H. ammodendron* in China. The *H. ammodendron* forest fixes a large amount of the quicksand around the oasis, which plays an important role in protecting the security of the oasis [10]. In recent years, due to the overexploitation and utilization of water resources, the groundwater level has dropped sharply, the process of desertification has accelerated, the *H. ammodendron* community has been seriously degraded, and a large area of death has developed [11,12], all of which seriously threaten oasis security and the ecological balance of the desert–oasis transition zone [13].

Many studies on the relationship between ecological hydrological processes and vegetation composition and climate have been carried out in the desert–oasis transition zone at the edge of the Gurbantunggut Desert [14–16]. Many scholars have evaluated the importance of groundwater for various types of vegetation and the effects of vegetation on groundwater decline [17–20]. However, this research has mostly been limited to vegetation with good soil water conditions [21], farmland crops that rely on irrigation and water replenishment [22–25], and riparian forest vegetation with river water replenishment [26,27]. There is a consensus concerning vegetation change under extreme drought conditions without irrigation or river water replenishment. Therefore, although the importance of soil water and shallow groundwater for vegetation in the desert–oasis transition zone has been recognized, estimations of the components of the water balance and the contribution rate of shallow groundwater to evapotranspiration are still lacking [28].

The importance of shallow groundwater for maintaining vegetation has been proposed in various water balance studies, which further underlines the importance of various ecosystems and crop systems for shallow groundwater [29]. As an important process of energy exchange between the land and atmosphere, evapotranspiration is also a key node in the water balance cycle [30]. The survival of vegetation in the desert–oasis transition zone mainly depends on precipitation, and more than 60% of precipitation returns to the atmosphere in the form of evaporation [31,32]. Evapotranspiration from shallow groundwater (ET_g) leads to significant losses in groundwater reserves [28,33,34]. When water moves upwards through capillarity to replenish soil water reserves, surface soil water storage is exhausted through surface evaporation and water absorption by the surface roots of vegetation. For crops, depths within 200 cm of the surface are usually effective [35–37], and the capillary rise rate increases with the development of crop roots. Therefore, it is reasonable to assume that the *H. ammodendron* forest in the desert–oasis transition zone can absorb soil water and shallow groundwater at depths of more than 200 cm below the surface due to the influence of root distribution [38].

Research on ET_g can be traced back to the beginning of the 20th century. The spatiotemporal variability of ET_g makes it difficult to estimate directly [39]. Research shows that soil moisture and groundwater level have certain memory effects on important ecological

hydrological processes (such as evapotranspiration and leakage processes) occurring in the aeration zone [40,41]. The question of how to use relatively convenient data and obtain a large amount of conventional observation data to estimate ET_g is a research hotspot and a new direction in ecology–hydrology, and there are still technical challenges [23,42]. As a typical hydrological method, the water balance method is widely used and has the advantages of low cost and high accuracy [43,44], but its credibility is poor in the desert–oasis transition zone, which has low precipitation and high evaporation intensity [45]. The groundwater level fluctuation method is mainly applicable for phreatic aquifers. It is not necessary to calculate the source and sink items for groundwater. Only the dynamic monitoring data for the regional groundwater level need to be used to obtain the total recharge of the region. Therefore, this method is practical and easy to employ in areas where the source and sink items are unknown and the data are incomplete [46,47].

Therefore, this study used Bowen ratio meteorological data, soil moisture data, and groundwater level fluctuation field monitoring data from the desert–oasis ecosystem at the Fukang National Experimental Station. The ET_g and its rate of contribution to the *H. ammodendron* shrub forest at the edge of the Gurbantunggut Desert were estimated with the water balance method and groundwater level fluctuation method, and the results can provide theoretical guidance and a scientific basis for water resource planning in the region.

2. Overview of the Study Area and Data

2.1. Overview of the Study Area

The Gurbantunggut Desert region is located in the northern part of Xinjiang (44°15′~46°50′ N, 84°50′~91°20′ E) and has an area of about 9.81 × 10^4 km^2 (Figure 1). The study area is a typical temperate desert climatic zone with important seasonal changes. Through an analysis of differing land uses and the vegetation cover gap between the Gurbantunggut Desert and northern Xinjiang (Table 1), it can be concluded that grassland and sparse vegetation represent the absolute gap. The sparse vegetation in the Gurbantunggut Desert area has the widest distribution area of about 9 × 10^4 km^2, accounting for 91.74% of the whole Gurbantunggut Desert area (Table 1). Through field investigations, it was found that the sparse vegetation mainly comprised *H. ammodendron* forest. The naturally occurring growth density of *H. ammodendron* is 0.25 plant·m^{-2}, the average diameter of the trees is 3.3 cm, the average height is 192 cm, the average width of the crowns is 199 cm × 192 cm, and the vegetation cover is 20~30%.

Table 1. Gap analysis of land use/land cover in Gurbantunggut Desert area in northern Xinjiang in 2020 (unit: 10^4 km^2).

Land Cover	Gurbantunggut Desert	Northern Xinjiang	Absolute Gap	Relative Gap
Tree cover	0.000,209	1.392,574	1.392,365	6663
Shrubland	0.011,053	0.380,542	0.369,489	34
Grassland	0.731,084	16.607,703	15.876,619	23
Cropland	0.051,919	4.151,747	4.099,828	80
Built-up	0.002,225	0.282,121	0.279,896	127
Bare/sparse vegetation	9.004,974	19.013,854	10.00,888	2
Snow and ice	0	0.309,646	0.309,646	-
Permanent water bodies	0.013,885	0.468,068	0.454,183	34
Herbaceous wetland	0.000,415	0.062,435	0.06,202	150
Moss and lichen	0.000,012	1.777,639	1.777,627	148,137

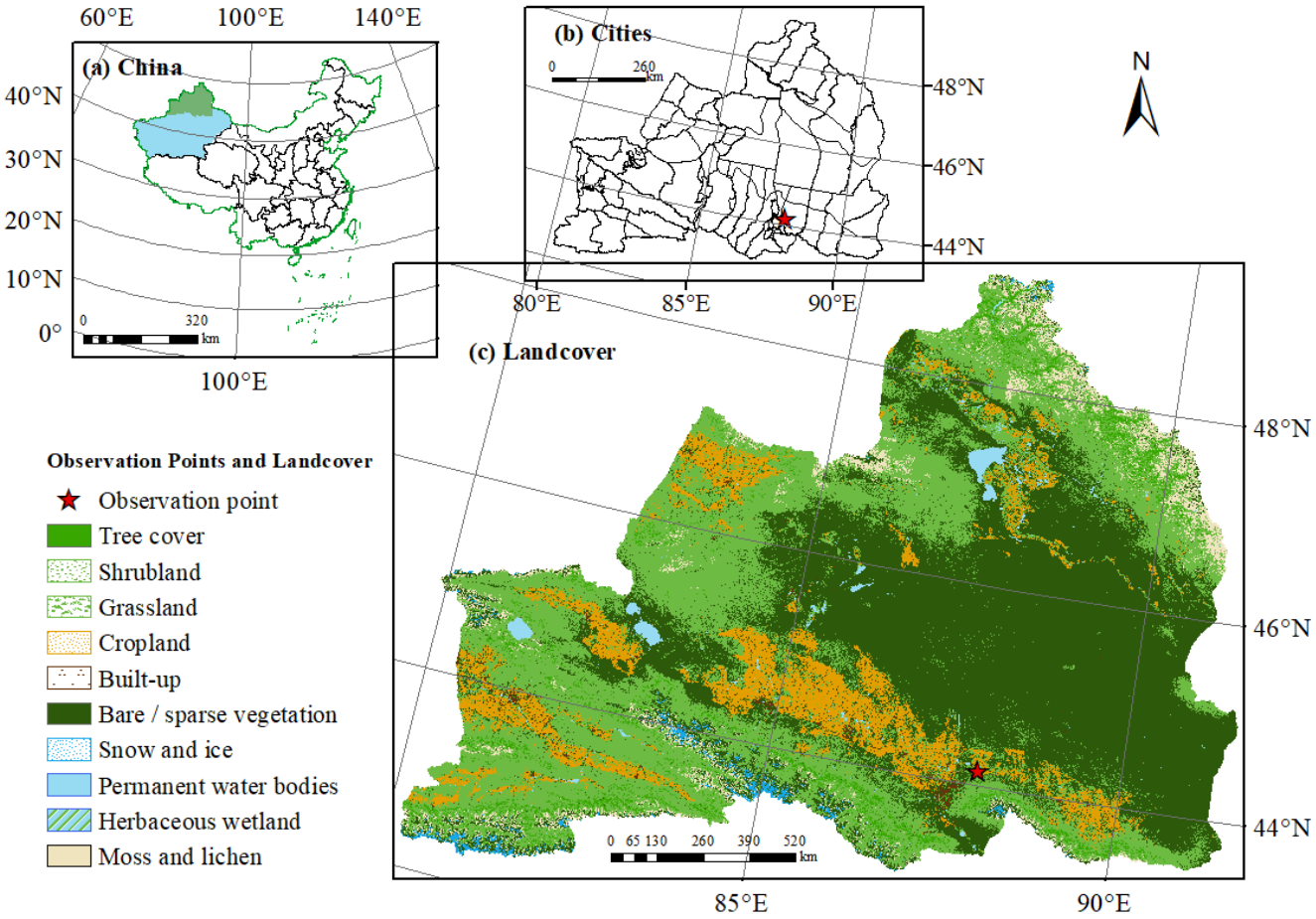

Figure 1. Map of China (**a**), City and County Map of Northern Xinjiang (**b**) and Landcover in Northern Xinjiang (ESA 10 m land cover data (**c**). Drawing review no.: GS (2020) no. 4619.

2.2. Data

From 2015 through 2018, soil moisture and Bowen ratio meteorological data for *H. ammodendron* shrubs were monitored at the Fukang Desert Ecosystem National Monitoring Station of the Chinese Academy of Sciences.

(1) Micrometeorological data for the Bowen ratio

Data were acquired with a CR1000X data collector (Campbell Scientific Inc., Logan, UT, USA). An NR-lite net radiometer (Campbell Scientific Inc., Logan, UT, USA) was used to measure Rn net radiation. An HMP45C (Campbell Scientific Inc., Logan, UT, USA) air temperature and humidity probe was used to measure the air temperature T and relative humidity RH at 3 m and 5 m. An HFP01SC soil heat flux plate (Campbell Scientific Inc., Logan, UT, USA) was used to measure the soil heat flux at 3 cm and 5 cm below the soil surface. The rainfall P and wind speed (2 m high position) data were monitored using an additional rainfall meter. The data were acquired once every 30 s, and the mean values were automatically saved every 30 min (Figure 2).

(2) Monitoring of soil moisture and *H. ammodendron* root system

Figure 3a shows the surface area distribution of *Haloxylon ammodendron* root system, and Figure 3b shows the soil moisture profile. Soil moisture was monitored automatically with a Hydra Plant Sensing (Aoda Plant Sensing Instruments Inc., Osborne, SA, Australia) instrument and a neutron detector, both at the roots of *H. ammodendron* shrubs (Figure 4). The Hydra soil moisture meter measures the soil moisture content of soil at depths of 10 cm, 30 cm, 50 cm, 70 cm, 90 cm, 110 cm, 130 cm, and 150 cm below the root surface by means of a pre-buried soil moisture probe. The automatic data acquisition instrument was connected to the probe by a cable, collected data every 5 s, and computed and stored the 10 min mean

values. Neutron monitoring of soil moisture was undertaken at depths of 30 cm, 50 cm, 70 cm, 90 cm, 110 cm, 130 cm, 150 cm, . . . , 950 cm, 970 cm, and 990 cm below the surface (Figure 3b). A total of 23 neutron tubes were buried at a depth of 1050 cm. Each layer was monitored three times, and the mean values were recorded. Soil moisture monitoring with a neutron tube was synchronized with groundwater monitoring, which started in early March each year and took place every 10 days. In this study, the multipoint curve fitting method was used to calibrate the soil sensor.

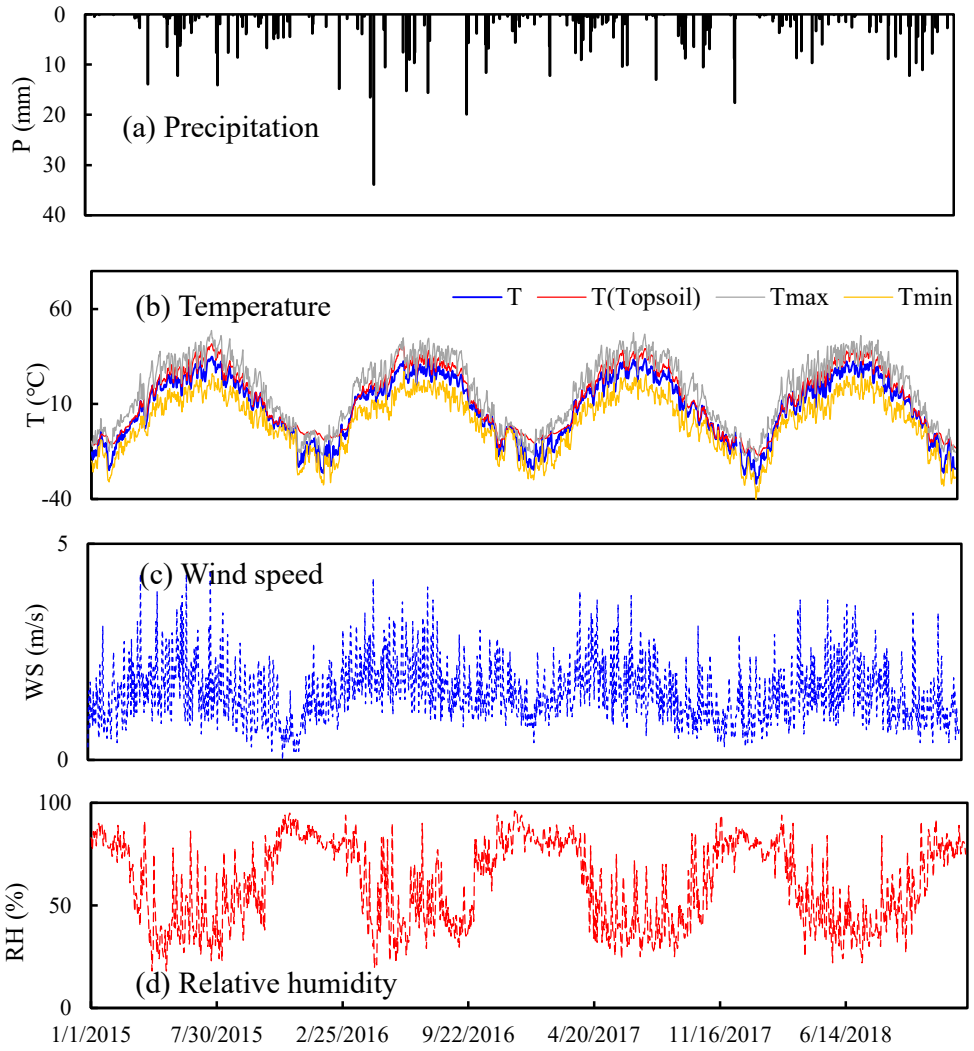

Figure 2. Precipitation (**a**), air temperature and soil temperature (**b**), wind speed (**c**), and relative humidity (**d**) in the study area from 2015 to 2018 (P, precipitation in mm/d; T, temperature in °C; WS, wind speed in m/s; RH, the relative humidity in %).

The *H. ammodendron* forest in the study area has developed roots. According to the layered excavation method, the root distribution range is 0~10 m, and the depth of the main roots reaches 8.33 m, with 66.6% of the roots being distributed in the 0~4 m soil layer (Figure 3a).

(3) Groundwater burial depth

Monitoring of the groundwater burial depth was primarily undertaken using a groundwater observation well constructed in advance approximately 0.5 m from the neutron tube (Figure 5). There were three groundwater observation wells: at the foot of the eastern slope, at the foot of the western slope, and in the bare earth between the hills. The heights of the control points were 400.95 m, 398.40 m, and 399.04 m, respectively. Figure shows the groundwater level fluctuation.

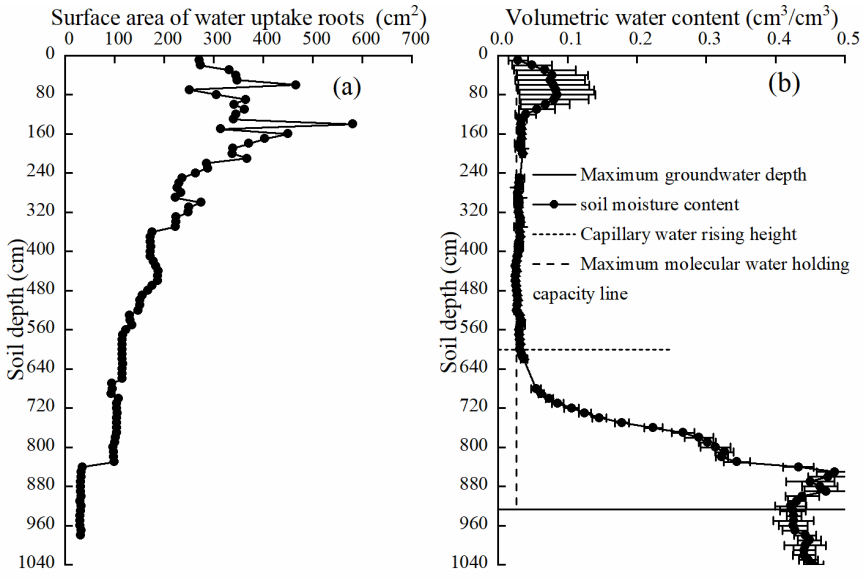

Figure 3. (**a**,**b**) Distribution of the *H. ammodendron* root system in the test area.

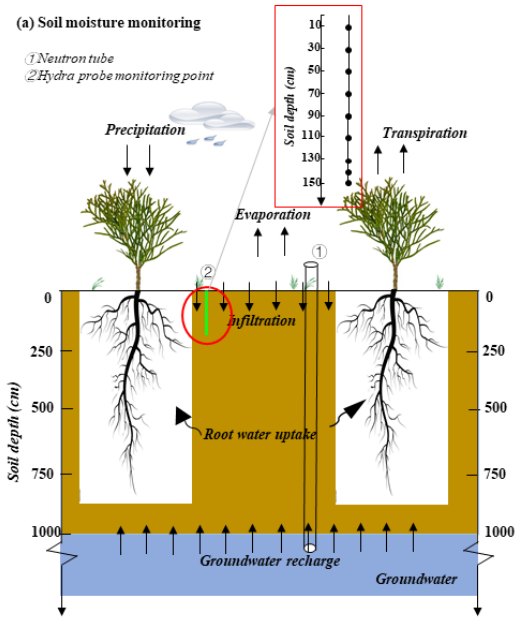

Figure 4. Monitoring of soil moisture in the *H. ammodendron* root zone.

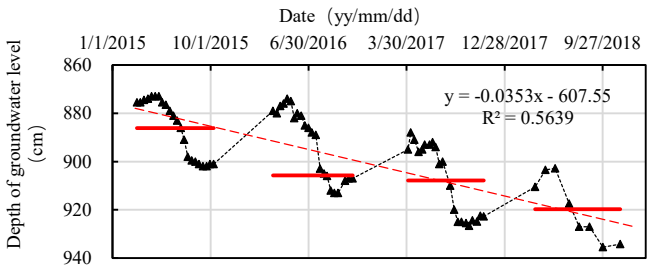

Figure 5. Dynamic diagram of groundwater burial depth. The red lines are the annual mean value for the groundwater depth, the red dotted line is the trend line for the annual groundwater level fluctuation, and the points represent the groundwater level monitoring depths.

3. Materials and Methods

3.1. Water Balance Method

The ET_0 reference evapotranspiration was computed using the FAO 56 Penman Monteith model [48]:

$$ET_0 = \frac{0.408\Delta(R_n - G) + \gamma\frac{900}{T+273}U_2(e_s - e_a)}{\Delta + \gamma(1 + 0.34U_2)} \quad (1)$$

where ET_0 is the reference evapotranspiration in mm day^{-1}, Rn is the net radiation in MJm^{-2}day^{-1}, G is the soil heat flux in MJm^{-2} day^{-1}, γ is the psychometric constant in kPa °C^{-1}), T is the mean air temperature in °C, U_2 is the wind speed at a 2 m height in m s^{-1}, e_s is the saturation vapour pressure in kPa, e_a is the actual vapour pressure in kPa, and Δ is the slope of the vapour pressure curve in kPa °C^{-1}.

(1) Energy balance method using the Bowen ratio

The energy balance method using the Bowen ratio can be used to indirectly estimate the sensible heat flux H and the latent heat flux λET of the canopy surface and then to obtain the actual evapotranspiration ET_a, which can be expressed as follows:

$$\lambda ET + H = R_n - G \quad (2)$$

$$\beta = \frac{H}{\lambda ET} = \gamma\frac{\Delta T}{\Delta e} \quad (3)$$

where β is the Bowen ratio, H is the sensible heat flux in MJ·m^{-2}·d^{-1}, λET is the latent heat flux in MJ·m^{-2}·d^{-1}, λ is the latent heat of vaporisation in MJ·kg^{-1}, ΔT is the two-stage air temperature difference in °C, and Δe is the two-stage air vapour pressure difference in kPa.

H and λET may be estimated using the following equations:

$$H = \frac{\beta}{(1+\beta)}(R_n - G) \quad (4)$$

$$\lambda ET = \frac{1}{(1+\beta)}(R_n - G) \quad (5)$$

where G is the soil heat flux in MJ·m^{-2}·d^{-1}, and Rn is the net radiation of the canopy surface in MJ·m^{-2}·d^{-1}.

(2) Water balance method

The groundwater in the desert–oasis transition zone is located at a deep level (>9 m). The average texture of the soil makes it ideal as a unit, and it shows no surface runoff or deep leakage. Based on water balance theory:

$$P + ET_g = ET_a + \Delta S \quad (6)$$

where P is the precipitation in the period in mm, ET_g is the evapotranspiration from groundwater in mm, ΔS is the soil water storage in the period in mm, and ET_a is the actual annual evapotranspiration in mm.

The accumulation of water in the soil ΔS is calculated as follows:

$$\Delta S = \sum_{i=1}^{n}(\theta_2 - \theta_1)_i \Delta d_i \quad (7)$$

where n is the number of layers from the effective root zone to the depths studied (0~1000 cm); θ_1 and θ_2 are the volumetric water contents of the first and second samplings, respectively, in m^3·m^{-3}; and Δd_i is the thickness of each soil layer in mm.

3.2. Water Table Fluctuation Method (WTF)

The groundwater level fluctuation method (WTF) is mainly used in arid and semiarid areas to estimate the ET_g for groundwater by analysing the groundwater level changes in unconfined aquifers [49,50]. The calculation formula is as follows:

$$ET_g = S_y \frac{\Delta H - \Delta h}{\Delta t} \tag{8}$$

where S_y is the specific yield, ΔH is the change in the groundwater table in the period in cm, Δh is the lateral runoff in cm, and Δt is the time interval in days.

Evapotranspiration of groundwater is caused by the combined action of soil evaporation and plant transpiration. The capillary rise flux of the groundwater table [51] is mainly affected by soil texture and the distribution of plant roots. According to this research, the upward flux of capillary water should eventually be consumed by evapotranspiration, regardless of lateral soil loss. Therefore, Equation (1) can be simplified to:

$$ET_g = S_y \frac{\Delta Z_y}{\Delta t} \tag{9}$$

where ΔZ_y is the seasonal decline in the groundwater table in cm.

The mean apparent specific yield Sya was used in this research, and it can be calculated from the parameters of the van Genuchten model [52]:

$$S_{ya} = S_{yu} - \frac{S_{yu}}{\left[1 + \left(\frac{z_i + z_f}{2}\right)^n\right]^{1-\frac{1}{n}}} \tag{10}$$

$$S_{yu} = \theta_r - \theta_s \tag{11}$$

where θ_s and θ_r are the saturated soil moisture content and residual soil moisture content in $cm^3 \cdot cm^{-3}$, respectively; z_i and z_f are the initial and final depths of the groundwater table in cm; and α and n are the parameters of the van Genuchten model. The model parameters are shown in Table 2.

Table 2. Basic physical parameters of soil.

Soil Depth (cm)	Soil Particle Size			Soil Texture	SBD	θ_r	θ_s	θ_c	θ_{fc}	θ_{hc}	α	n	Ks
	Clay (0~0.002 mm)	Silt (0.002~0.05)	Sand (0.05~2 mm)										
0~20	1.08	5.76	93.16		1.58	0.0465	0.3827	0.38	0.22	0.02	0.0376	3.1716	582.70
20~40	1.63	12.31	86.06		1.58	0.0390	0.3888	0.38	0.23	0.02	0.0435	2.2.48	208.71
40~60	1.10	6.90	92.00		1.58	0.0452	0.3840	0.39	0.26	0.03	0.0386	2.9900	491.38
60~80	1.21	7.07	91.72	Sand	1.53	0.0451	0.3840	0.39	0.26	0.03	0.0387	2.9415	470.20
80~100	1.23	7.07	91.71		1.56	0.0451	0.3840	0.39	0.26	0.03	0.0387	2.9384	468.97
100~150	1.23	8.79	89.88		1.50	0.0429	0.3857	0.41	0.29	0.03	0.0403	2.6814	359.66
Average	1.26	7.98	90.76		1.56	0.0440	0.3849	0.39	0.25	0.03	0.0376	3.1716	582.70

Note(s): *SBD* is the dry bulk density of soil in $g \cdot cm^{-3}$; θ_r is the residual soil moisture content in $cm^3 \cdot cm^{-3}$; θ_s is the saturated moisture content of soil in $cm^3 \cdot cm^{-3}$; θ_c is the capillary water holding capacity in $cm^3 \cdot cm^{-3}$; θ_{fc} is the field water holding capacity in $cm^3 \cdot cm^{-3}$; θ_{hc} is the moisture absorption coefficient in $cm^3 \cdot cm^{-3}$; α is a parameter in the soil water characteristic function in cm^{-1}; n is another parameter in the soil moisture characteristic function; *Ks* is the saturated hydraulic conductivity in $cm \cdot day^{-1}$.

Equation (10) was used to calculate the average apparent specific yield S_{ya}. When the groundwater table fluctuates in the 0–10 m soil layer, the soil temperature increases.

$$\overline{S_{ya}} = \frac{\sum_{i=1}^{m} \Delta h_i S_{yi}}{\sum_{i=1}^{m} \Delta h_i} \quad i = 1, 2, \ldots, m \tag{12}$$

where S_{yi} is the specific yield of the corresponding soil layer and Δh_i is the fluctuation amplitude of the groundwater table in the i-th layer in cm.

Soil texture affects the water yield S_y and thus the accuracy of the ET_g estimation in the *WTF* model [27,53]. Therefore, we considered the impacts of different soil textures on water yield S_y, as shown in Table 3.The soil texture in the study area was mainly sandy.

Table 3. Water contents of different soil textures.

Soil Type	$\theta_s - \theta_r$	Depths Compensated	S_y
Sand	0.391	0.35–0.36	0.47
Sandy loam	0.345	0.31–0.32	0.38
Loam	0.352	0.24–0.25	0.25
Silt loam	0.383	0.18–0.19	0.19
Silt	0.426	0.16–0.18	0.16

3.3. Data Preprocessing and Model Evaluation

3.3.1. Data Preprocessing

The accuracy β of the Bowen specific energy balance method determines its accuracy in estimating the latent heat flux β. When it approaches -1, the λET tends to infinity, which has no practical physical significance. Therefore, the calculation of latent heat flux λET using the measured Bowen ratio required data preprocessing and the selection of the Bowen ratio data. Research shows that the unreasonable data range for the value of β is dynamic [54] and mainly related to the water pressure gradient and the resolution of the sensor. Under the condition that the energy flux directionality of the Bowen ratio data is correct, the accuracy of the temperature and humidity probes can be used to construct the β value, and the dynamic rejection field β error limit is ε; thus, we obtain:

$$\varepsilon = \delta\beta = \left|\frac{\partial\beta}{\partial\Delta T}\right|\delta\Delta T + \left|\frac{\partial\beta}{\partial\Delta e}\right|\delta\Delta e = \left|\frac{\gamma}{\Delta e}\right|\delta\Delta T + \left|-\gamma\frac{\Delta T}{(\Delta e)^2}\right|\delta\Delta e \tag{13}$$

When β is close to -1, it can be seen that:

$$\varepsilon \approx \left|\frac{\delta\Delta e + \gamma\delta\Delta T}{\Delta e}\right| \tag{14}$$

The accuracies of the temperature and humidity probes used in this study ($\delta\Delta T$ and $\delta\Delta e$) were 0.1 °C and 0.02 kPa, respectively. Thus:

$$\varepsilon = \left|\frac{0.0026}{\Delta e}\right| \tag{15}$$

Therefore, the $\beta = -1 \pm \varepsilon$ functions constitute β as shown in the figure; the shaded part represents the β value rejection field. As can be seen from Figure 6, the β value rejection domain mainly changes due to changes in the water pressure gradient Δe. When $\Delta e \to 0$, β is larger in the reject field near -1.

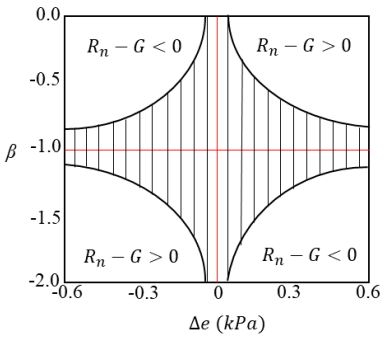

Figure 6. Rejection domain dynamic graph.

3.3.2. Model Validation

In this research, the correlation coefficient (R), root-mean-square error ($RMSE$), bias, and index of agreement (IOA) were used to estimate the performance of the actual evapotranspiration model.

$$R = \frac{\sum_{i=1}^{N}(M_i - \overline{M})(G_i - \overline{G})}{\sqrt{\sum_{i=1}^{N}(M_i - \overline{M})^2}\sqrt{\sum_{i=1}^{N}(G_i - \overline{G})^2}} \quad (16)$$

$$RMAE = \sqrt{\frac{\sum_{i=1}^{N}(M_i - G_i)^2}{N}} \quad (17)$$

$$BIAS = \frac{\sum_{i=1}^{N}(M_i - G_i)}{N} \quad (18)$$

$$IOA = 1 - \frac{\sum_{i=1}^{N}(M_i - G_i)^2}{\sum_{i=1}^{N}(|M_i - \overline{G}| + |G_i - \overline{G}|)^2} \quad (19)$$

where M_i and G_i are the estimated value and the measured value in the model, respectively; the subscript i indicates the i-th sample; N is the total number of data pairs in the study period; and $\overline{M}$ and $\overline{G}$ are the means of the estimated values and the measured values in the model, respectively.

4. Results and Analysis

4.1. Meteorological Conditions and Observation Data

4.1.1. Meteorological Conditions

According to the in situ observation of Bowen ratio meteorological data in the study area, the annual mean P for the studied years was 177.93 mm, and the average annual P in the main growth season was 126.58 mm (Figure 2a), representing 70.84% of the yearly average precipitation. The rainfall was unevenly distributed in time. The interannual high temperature T_{max} was 48.74 °C, the extreme low temperature T_{min} was −44.11 °C, and the annual mean temperature T was 8.15 °C. The surface soil temperature in the study area was usually above the average temperature, and the annual average surface soil temperature $T_{(topsoil)}$ was 12.43 °C (Figure 2b). The annual mean wind speed at 2 m WS was 1.55 m/s, with a maximum wind speed WS of 4.4 m/s (Figure 2c). The trends for the air temperature, surface soil temperature, and wind speed in the study area were consistent, showing a unique peak curve throughout the year. Relative humidity RH showed a trend opposite to those of air temperature, surface soil temperature, and wind speed, with the peak appearing in December each year (Figure 2d).

4.1.2. Distribution of the *Haloxylon ammodendron* Root System

The *H. ammodendron* forest in the study area has developed roots. According to the layered excavation method, the root distribution range is 0~10 m, and the depth of the main roots reaches 8.33 m, with 66.6% of the roots being distributed in the 0~4 m soil layer (Figure 4a). The surface *H. ammodendron* roots mainly absorb the soil water transformed by precipitation infiltration, while the deeper taproot distribution provides conditions for the development of deep absorption roots (root diameter < 2 mm), which in turn provides the conditions for *H. ammodendron* vegetation to use groundwater. Moreover, some studies have shown that, when the groundwater level drops, *H. ammodendron* continues to extend downwards to ensure its survival due to its water-seeking tendency [10,54]. Xu and Li [5] noted that, when the groundwater depth was 18 m, the distribution of the water-absorbing roots of *H. ammodendron* could still be observed with the excavation method.

4.1.3. Soil Water Capillarity Support

Soil capillary action drives the movement from groundwater to soil water. The rise height of the capillary determines whether the capillary water can recharge the soil layers available to plants, directly affecting the survival of desert vegetation [8,9]. Soil water capillarity support is the only way for soil to be supplied with groundwater. From the determination of the intersection position of the maximum molecular water capacity line and the average soil moisture content of the profile, the maximum rise height of the capillary water was judged to be 600 cm (Figure 4b). In the distribution range of the *H. ammodendron* root system, although less precipitation can penetrate into the middle and deep layers of the soil and the level of infiltration of surface precipitation is low, *H. ammodendron* can still absorb the water in the soil through its strong root system via the support of capillarity (Figure 4). This finding is consistent with the conclusion provided by Xu et al. [35]; that is, the distribution of vegetation roots affects capillarity, allowing *H. ammodendron* vegetation to absorb shallow groundwater and survive.

4.1.4. Groundwater Depth Fluctuation

Groundwater is considered the main water source for desert vegetation growth in arid areas [17–20]. The interannual groundwater depth in the study area decreased in a fluctuating manner. From 2015 to 2018, the groundwater depth decreased by an average of 11.21 cm per year, and the maximum decline increased to 15.75 cm per year (Figure 5). The main period of groundwater consumption in the year is from May to October, and the period of groundwater recharge is from October to May of the following year (Figure 5). The recovery of groundwater depth was found to be mainly achieved through the melting and recharge of snow in winter and the lateral recharge from farmland flood irrigation in spring and winter near the desert–oasis transition zone, which is consistent with the conclusions of other scholars [55,56]. The period of decline for the groundwater depth is mainly from May to October. The reason for the decline is that this period is the main growing season for vegetation. The evapotranspiration associated with vegetation is strong. The main water source for vegetation is groundwater. ET_g leads to significant losses of groundwater reserves. When the water moves upwards from the capillary zone, it supplements the soil water reserves. At this time, soil water storage becomes exhausted through surface evaporation and root water absorption [8,9].

4.2. β Value Exclusion Domain

After calculation and screening of λET and H with the Bowen Ratio Data Screening Program in MATLAB software, the total numbers of micrometeorological data samples for the Bowen ratio in 2015, 2016, 2017, and 2018 were 52,561, 51,912, 52,552, and 56,880, respectively. There was some missing data for the weather monitoring over the year, and the data qualification rates were 81.82%, 77.50%, 76.37%, and 78.4%, respectively (Table 4). Finally, the eliminated data were supplemented using a linear interpolation formula; accurate Bowen ratio data could be obtained, and the energy balance closure for the filtered data was significantly improved.

Table 4. β value rejection domain types and data disqualification rates.

Type	β Value Exclusion Domain			2015		2016		2017		2018	
				a	*b* (%)	*a*	*b* (%)	*a*	*b* (%)	*a*	*b* (%)
A	$Rn - G > 0$	$\Delta e > 0$	$\beta < -1 + \lvert\varepsilon\rvert$	1556	2.96	959	1.85	2041	3.97	370	1.2
B	$Rn - G > 0$	$\Delta e < 0$	$\beta > -1 + \lvert\varepsilon\rvert$	2905	5.53	6277	12.09	1615	3.14	958	3.11
C	$Rn - G < 0$	$\Delta e > 0$	$\beta > -1 - \lvert\varepsilon\rvert$	4586	8.73	3564	6.87	8473	16.48	4945	16.05
D	$Rn - G < 0$	$\Delta e < 0$	$\beta < -1 + \lvert\varepsilon\rvert$	508	0.97	882	1.70	23	0.04	26	0.08
Amounting to				9555	18.18	11,682	22.50	12152	23.63	6656	21.6

Note(s): *a* indicates the number of nonconforming data samples and *b* the nonconforming rate.

4.3. Energy Balance and Evapotranspiration

4.3.1. Energy Composition and Proportions

The Bowen ratio closed better than the energy balance after data screening [49], which provided the conditions for the subsequent accurate calculation of the important term in the water balance—the actual evapotranspiration ET_a.

The energy components of the shuttle were different in different growth and development periods. The peak latent heat flux λET and net radiation R_n appeared in the summer dormancy period, and a trend for the sensible heat flux was not obvious in any of the growth periods. The negative value for the soil heat flux G in the late stage of branch growth indicated that the soil heat released to the atmosphere began to freeze [57]. The proportions of the energy budget in the growing season were as follows: latent heat flux > sensible heat flux > soil heat flux. As an important component of the energy flux, latent heat was the main contributor to water consumption in the growing season [58,59], with its energy balance accounting for 70.16~91.86%, while the sensible heat flux energy balance accounted for 15.80~33.52%. The proportions of soil heat flux were −15.47~9.377% (Table 5).

Table 5. The change in energy flux during the phenophase of *H. ammodendron* in 2015–2016. R_n is the net radiation, λET is the latent heat flux, H is the sensible heat flux, and G is the geothermal flux.

Years	Phenological Period	Time Slot	Days	Energy Component (MJ· m^{-2}·d^{-1}				Proportion of Energy Balance (%)			β
				H	*λET*	*Rn*	*G*	*H/Rn*	*λET/Rn*	*G/Rn*	
2015	Early budding	12 April–22 April	11	22.01	68.85	98.13	7.27	22.43	70.16	7.41	4.97
	Budding	23 April–30 April	8	18.81	67.70	94.36	7.85	19.93	71.75	8.32	1.90
	Assimilating branch growth	1 May–14 May	15	17.26	68.20	94.31	8.84	18.30	72.31	9.37	1.92
	Late summer dormancy	15 May–24 September	132	20.22	91.16	116.28	4.89	17.39	78.40	4.21	1.33
	Late shoot growth	25 September–29 October	25	8.31	48.31	52.59	−4.03	15.80	91.86	−7.66	2.1
2016	Early budding	18 May–2 May	15	21.51	68.04	94.68	5.13	22.72	71.86	5.42	4.15
	Budding	3 May–12 May	10	17.36	68.90	91.76	5.50	18.92	75.09	5.99	2.01
	Assimilating branch growth	13 May–22 May	10	19.40	77.95	101.9	4.55	19.04	76.50	4.47	1.94
	Late summer dormancy	23 May–10 October	141	20.10	88.34	112.79	4.35	17.82	78.32	3.86	1.26
	Late shoot growth	11 October–2 November	23	15.14	37.02	45.17	−6.99	33.52	81.96	−15.47	3.69

4.3.2. Evapotranspiration

The precipitation in the main growing season of the vegetation in the study area was low, and the evapotranspiration was high. The annual average potential evapotranspiration reached as high as 1237.50 mm, while the annual average actual evapotranspiration ET_a was 260.87 mm, and the annual precipitation accounted for 68.21% of the actual evapotranspiration (Figure 7). Precipitation cannot meet the needs of desert vegetation growth [54]. Therefore, in desert–oasis transition zones without irrigation or water replenishment, groundwater is considered to be important for the survival of vegetation [18,20]. However, this is only true for deep-rooted vegetation, such as shuttles; furthermore, in June and July, when the temperature is relatively hot, plants with shallow roots die [16]. Other scholars have also noted that short-lived plants are significantly affected by precipitation and that groundwater evapotranspiration has no significant effect on plants with shallow roots [38].

4.4. Groundwater Evapotranspiration

The water balance method and groundwater level fluctuation method were used to estimate the evapotranspiration ET_g for *H. ammodendron* vegetation from groundwater. The validation accuracy R of the model was greater than 0.96, the *RMSE* range was 1.5931~4.5706, the bias range was −0.15~−0.11, and the *IOA* value was greater than 0.95. The model estimation accuracy was high (Table 6).

Table 7 shows the components of the water balance during the growth period of *H. ammodendron*. The annual average value for the actual evapotranspiration ET_a during the growth period of *H. ammodendron* was 244.32 mm, the annual average value of precipitation in the growth period was 145.24 mm, and the precipitation accounted for 59.44%

of the actual evapotranspiration. The average annual value for ET_g from groundwater evapotranspiration in the growth period was 182.35 mm (Table 7), and the contribution rate for groundwater reached up to 74.78%. The results of the water balance method were relatively underestimated compared to those of the *WTF* model. In summary, it was concluded that groundwater is an important component of the water balance in the desert–oasis transition zone and the main water source for the growth and survival of *H. ammodendron* vegetation [12,25,60].

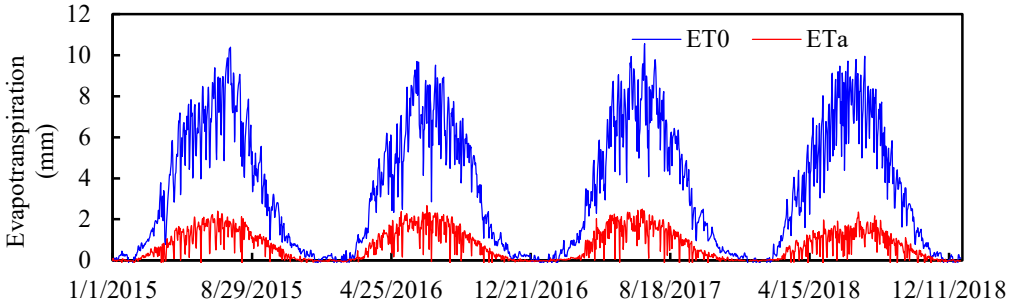

Figure 7. Reference evapotranspiration ET_0 and actual evapotranspiration ET_a for *H. ammodendron* vegetation.

Table 6. Verification of ET_g using water balance method and groundwater level fluctuation method (*WTF*).

Year	Phenological Period	Validation Indicators			
		R	RMAE	Bias	IOA
2015	Early budding	0.9780	4.5706	−0.15	0.9585
	Budding	0.9669	2.1989	−0.11	0.9507
	Assimilating branch growth	0.9718	4.5657	−0.11	0.9548
	Late summer dormancy	0.9771	2.7667	−0.14	0.9831
	Late shoot growth	0.9683	3.6789	−0.11	0.9654
2016	Early budding	0.9646	3.7134	−0.12	0.9771
	Budding	0.9703	2.3849	−0.12	0.9688
	Assimilating branch growth	0.9713	2.4510	−0.14	0.9719
	Late summer dormancy	0.9654	3.2468	−0.13	0.9570
	Late shoot growth	0.9638	1.5931	−0.11	0.9892

Table 7. Water balance in the *H. ammodendron* growth period.

Year	Phenological Period	Time Slot	Days	*P* (mm)	ET_0 (mm)	ET_a (mm)	ΔS (mm)	ET_g (mm)	ET_g (*WTF*) (mm)
2015	Early budding	12 April–22 April	10	14.0	49.11	11.53	43.82	41.35	44.1
	Budding	23 April–30 April	8	0.0	45.81	8.97	37.92	46.89	49.4
	Assimilating branch growth	1 May–14 May	15	0.5	85.34	15.64	32.54	47.68	48.11
	Late summer dormancy	15 May–24 September	132	97.5	874.97	189.54	−79.81	12.23	13.38
	Late shoot growth	25 September–29 October	25	13.0	71.78	16.71	23.81	27.52	27.09
Total			190	125	1127.02	242.38	58.28	175.67	182.08
2016	Early budding	18 May–2 May	14	50.4	65.74	17.11	56.07	22.78	23.56
	Budding	3 May–12 May	10	0.0	54.34	15.66	40.39	56.05	60.01
	Assimilating branch growth	13 May–22 May	10	13.6	55.36	17.02	41.51	44.93	45.27
	Late summer dormancy	23 May–10 October	141	97.6	849.69	190.90	−76.82	16.48	18.77
	Late shoot growth	11 October–2 November	23	3.8	25.89	5.57	39.32	41.09	44.12
Total			198	165.47	1051.02	246.26	100.47	181.33	191.73

5. Discussion

5.1. Error Analysis

The error sources for the Bowen ratio energy balance method include: (1) Errors in $R_n - G$. The observation accuracy for $R_n - G$ is mainly reflected in the measurement accuracy for R_n. When we control the observation accuracy for ΔT and Δe, we can ensure that the calculation errors generated by them are as small as possible, so the observation accuracy for $R_n - G$ must be strictly controlled and must be kept within 5~10%; (2) ΔT and Δe observation errors. If the accuracy of the temperature and humidity gradienter is improved to $\sigma\Delta T$ = 0.05 °C and $\sigma\Delta e$ = 0.05 hPa, the calculation error in the Bowen energy balance model can be greatly reduced under conditions of non-advection or advection inversion; (3) The turbulence exchange coefficient (K_H) and water vapour exchange coefficient (K_W). The most basic assumption of the general Bowen ratio energy balance model is currently $K_H = K_W$. Although a large number of studies suggest that $K_H = K_W$, there are also studies that show that $K_H < K_W$ under stable conditions; (4) The influence of the length of the wind wave zone under advection and inversion conditions. The wind wave zone refers to the length range of the horizontal uniformity in the windward direction from the observation point. It is generally believed that the length of the wind wave zone should be more than 100 times the installation height of the temperature and humidity sensor and anemometer.

5.2. Uncertainty Analysis

The uncertainty analysis was undertaken by calculating the relative error limit of ET_a. For the effects of $R_n - G$ and β on the measured evapotranspiration value, it was assumed that the error caused by R_n was 5% R_n, and the error caused by G was 30% G [55].

$$\delta\beta = \left|\frac{\partial\beta}{\partial\Delta T}\right|\delta\Delta T + \left|\frac{\partial\beta}{\partial\Delta e}\right|\delta\Delta e = \left|\frac{\gamma}{\Delta e}\right|\delta\Delta T + \left|-\gamma\frac{\Delta T}{(\Delta e)^2}\right|\delta\Delta e = |\beta|\left(\frac{\delta\Delta T}{|\Delta T|} + \frac{\delta\Delta e}{|\Delta e|}\right) \quad (20)$$

$$\frac{\delta\beta}{|\beta|} = \frac{\delta\Delta T}{|\Delta T|} + \frac{\delta\Delta e}{|\Delta e|} \quad (21)$$

$$\frac{\delta R_n + \delta G}{|R_n - G|} = \frac{0.05R_n + 0.3G}{|R_n - G|} \quad (22)$$

$$\frac{\delta ET}{ET} = \frac{\delta R_n + \delta G}{|R_n - G|} + \frac{\delta\beta}{|1 + \beta|} \quad (23)$$

The Bowen ratio energy balance method is an indirect method for calculating latent heat flux, and its accuracy is affected by $R_n - G$. The uncertainty of $R_n - G$ was analysed by calculating the relative error limit for the available energy, as shown in Figure 8. Between 6:00 and 20:00 in the daytime, the relative uncertainty of $R_n - G$ was below 50%; the uncertainty at noon was about 20% and that at 18:00 was only 10%. The uncertainty at night was greater than 100%, making it unfavourable for the accurate determination of evapotranspiration. The change rule for ET_a uncertainty is consistent with that for $R_n - G$ uncertainty. It can be seen that whether $R_n - G$ can be accurately measured determines the measurement accuracy for ET_a to a certain extent. According to the uncertainty analysis for β, during the day (11:00~16:00), the uncertainty was less than 20%, and at night, it increased to about 40%. The uncertainty of β had two peaks in the morning (8:00) and evening (20:00) at respectively 65% and 56%. During those times, the uncertainty of β had a great impact on the uncertainty of ET_a, which restricted the accurate estimation of ET_a.

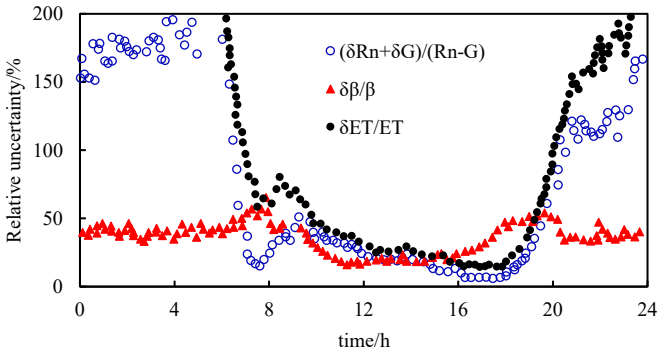

Figure 8. Uncertainty analysis for the determination of *ET* using the Bowen ratio energy balance method.

6. Summary and Conclusions

The Bowen specific energy closure after data screening was high, and the calculated annual ET_a value was relatively reliable, with a value of 260.87 mm. As the main contributor to water consumption in the growing season, latent heat accounted for 70.16~91.86% of the energy balance. The study found that precipitation had no significant impact on water consumption for *H. ammodendron* vegetation growth, and the precipitation in the main growing season accounted for 59.44% of the ET_a. From 2015 to 2018, the groundwater depth in the study area showed a decreasing trend each year, and the groundwater depth had a significant impact on the growth of *H. ammodendron* vegetation. Although the groundwater depth in the study area was greater than 9 m, ET_g, as an important part of the water balance, participated in the evapotranspiration process associated with the *H. ammodendron* forest due to the strong root system and supporting capillary water in the soil. The actual evapotranspiration ET_a in the desert–oasis transition zone in the main growing season was 244.32 mm, and the contribution rate for ET_g was as high as 74.78% or approximately 182.35 mm.

In the verification of ET_g using the water balance method and the groundwater level fluctuation method (*WTF*), R was greater than 0.96, the *RMSE* range was 1.5931~4.5706, the bias range was −0.15~0.11, and the *IOA* value was greater than 0.95. The accuracy of the estimation model was high, and the results were relatively accurate. The Bowen energy balance method has better applicability for *H. ammodendron* forests in transitional desert–oasis zones. The model can be applied in desert–oasis transition zones to obtain accurate ET_g estimations and can provide theoretical guidance and a scientific basis for local water resource management and ecological protection.

Author Contributions: Conceptualization, P.J. and S.-J.H.; methodology, P.J.; software, P.J.; validation, P.J.; formal analysis, P.J.; investigation, P.J. and S.-J.H.; resources, S.-J.H.; data curation, P.J. and S.-J.H.; writing—original draft preparation, P.J.; writing—review and editing, P.J. and S.-J.H.; supervision, S.-J.H. All authors have read and agreed to the published version of the manuscript.

Funding: This work was supported by the National Key R&D Program of China (no. 2021YD1900801), the National Natural Science Foundation of China (no. 41671032), and the special fund project of Xinjiang Water Conservancy Science and Technology (nos YF2020-08 and XSKJ-2021-05).

Institutional Review Board Statement: Not applicable.

Informed Consent Statement: Not applicable.

Data Availability Statement: Data are contained within the article.

Conflicts of Interest: The authors declare no conflict of interest.

References

1. Ullah, I.; Saleem, F.; Iyakaremye, V.; Yin, J.; Ma, X.Y.; Syed, S.; Hina, S.; Temesgen, G.A.; Omer, A. Projected Changes in Socioeconomic Exposure to Heatwaves in South Asia Under Changing Climate. *Earth's Future* **2022**, *10*, e2021EF002240. [CrossRef]
2. Iyakaremye, V.; Zeng, G.; Ullah, I.; Gahigi, A.; Mumo, R.; Ayugi, B. Recent Observed Changes in Extreme High-Temperature Events and Associated Meteorological Conditions over Africa. *Int. J. Climatol.* **2021**, *42*, 4522–4537. [CrossRef]
3. Zin, M.M.S.; Ullah, I.; Syed, S.; Zhi, X.F.; Azam, K.; Rasool, G. Interannual Variability of Air Temperature over Myanmar: The Influence of ENSO and IOD. *Climate* **2021**, *9*, 35. [CrossRef]
4. Zin, M.M.S.; Ullah, I.; Saleem, F.; Zhi, X.F.; Syed, S.; Azam, K. Interdecadal Variability in Myanmar Rainfall in the Monsoon Season (May–October) Using Eigen Methods. *Water* **2021**, *13*, 729. [CrossRef]
5. Zin, M.M.S.; Zhi, X.F.; Ullah, I.; Azam, K.; Ngoma, H.; Saleem, F.; Xing, Y.; Iyakaremye, V.; Syed, S.; Hina, S.; et al. Recent variability of sub-seasonal monsoon precipitation and its potential drivers in Myanmar using in-situ observation during 1981–2020. *Int. J. Climatol.* **2021**, *42*, 3341–3359. [CrossRef]
6. Yin, X.W.; Feng, Q.; Zheng, X.J.; Zhu, M.; Wu, X.; Guo, Y.; Wu, M.; Li, Y. Spatio-temporal dynamics and eco-hydrological controls of water and salt migration within and among different land uses in an oasis-desert system. *Sci. Total Environ.* **2021**, *772*, 145572. [CrossRef]
7. Yin, X.W.; Feng, Q.; Li, Y.; Deo, R.C.; Liu, W.; Zhu, M.; Zheng, X.J.; Liu, R. An interplay of soil salinization and groundwater degradation threatening coexistence of oasis-desert ecosystems. *Sci. Total Environ.* **2022**, *806*, 150599. [CrossRef]
8. Kahlown, M.A.; Ashraf, M.; ZiaulHaq. Effect of shallow groundwater table on crop water requirements and crop yields. *Agric. Water Manag.* **2005**, *76*, 24–35. [CrossRef]
9. Soylu, M.E.; Kucharik, C.J.; Loheide, S.P., II. Influence of groundwater on plant water use and productivity: Development of an integrated ecosystem-variably saturated soil water flow model. *Agric. Forest Meteorol.* **2014**, *189–190*, 198–210. [CrossRef]
10. Xu, G.Q.; Li, Y. Rooting depth and leaf hydraulic conductance in the xeric tree Haloxyolon ammodendron growing at sites of contrasting soil texture. *Funct. Plant Biol.* **2008**, *35*, 1234–1242. [CrossRef]
11. Ma, X.D.; Fan, L.M.; Yan, G.; Li, W.L. Vegetation responses to groundwater level change in mining area. *J. China Coal Soc.* **2017**, *42*, 44–49. (In Chinese) [CrossRef]
12. Lowry, C.S.; Loheide, S.P., II; Moore, C.E.; Lundquist, J.D. Groundwater controls on vegetation composition and patterning in mountain meadows. *Water Resour. Res.* **2011**, *47*, 896–898. [CrossRef]
13. Zhou, H.F.; Wu, B.; Wang, Y.G.; Li, Y. Ecological achievement of Xinjiang production and construction corps and its problems and countermeasures. *Bull. Chin. Acad. Sci.* **2017**, *22*, 55–63.
14. Zhao, R.M.; Hui, R.; Liu, L.C.; Xie, M.; An, L.Z. Effects of snowfall depth on soil physical-chemical properties and soil microbial biomass in moss-dominated crusts in the Gurbantunggut Desert, Northern China. *Catena* **2018**, *169*, 175–182. [CrossRef]
15. Xie, J.B.; Liu, T. Characterization of spatial scaling relationships between vegetation pattern and topography at different directions in Gurbantunggut desert, China. *Ecol. Complex.* **2010**, *7*, 234–242. [CrossRef]
16. Peng, M.W.; He, H.; Wang, Z.K.; Li, G.F.; Liu, X.H.; Pu, X.Z.; Zhuang, L. Responses and comprehensive evaluation of growth characteristics of ephemeral plants in the desert–oasis ecotone to soil types. *J. Environ. Manag.* **2022**, *316*, 115288. [CrossRef]
17. Xu, X.; Liu, H.; Jiao, F.; Gong, H.; Lin, Z. Time-varying trends of vegetation change and their driving forces during 1981–2016 along the silk road economic belt. *Catena* **2020**, *195*, 104796. [CrossRef]
18. Liu, B.; Guan, H.D.; Zhao, W.Z.; Yang, Y.T.; Li, S.B. Groundwater facilitated water-use efficiency along a gradient of groundwater depth in arid northwestern China. *Agric. Forest Meteorol.* **2017**, *233*, 235–241. [CrossRef]
19. Chen, H.S.; Hu, K.; Nie, Y.P. Analysis of soil water movement inside a foot slope and a depression in a karst catchment. *Sci. Rep.* **2017**, *7*, 2544. [CrossRef]
20. Sprenger, M.; Tetzlaff, D.; Soulsby, C. Soil water stable isotopes reveal evaporation dynamics at the soil-plant-atmosphere interface of the critical zone. *Hydrol. Earth Syst. Sci.* **2017**, *21*, 3839–3858. [CrossRef]
21. Fan, J.L.; Oestergaard, K.T.; Guyot, A.; Lockington, D.A. Estimating groundwater recharge and evapotranspiration from water table fluctuations under three vegetation covers in a coastal sandy aquifer of subtropical Australia. *J. Hydrol.* **2014**, *519*, 1120–1129. [CrossRef]
22. Boyko, K.; Fernald, G.D.; Bawazir, A.S. Improving groundwater recharge estimates in alfalfa fields of New Mexico with actual evapotranspiration measurements. *Agric. Water Manag.* **2021**, *244*, 106532. [CrossRef]
23. Wang, X.W.; Huo, Z.L.; Feng, S.Y.; Guo, P.; Guan, H.D. Estimating groundwater evapotranspiration from irrigated cropland incorporating root zone soil texture and moisture dynamics. *J. Hydrol.* **2016**, *543*, 501–509. [CrossRef]
24. Wu, Y.; Liu, T.; Paredes, P.; Duan, L.; Pereira, L.S. Water use by a groundwater dependent maize in a semi-arid region of Inner Mongolia: Evapotranspiration partitioning and capillary rise. *Agric. Water Manag.* **2015**, *152*, 222–232. [CrossRef]
25. Babajimopoulos, C.; Panoras, A.; Georgoussis, H.; Arampatzis, G.; Hatzigiannakis, E.; Papamichail, D. Contribution to irrigation from shallow water table under field conditions. *Agric. Water Manag.* **2007**, *92*, 205–210. [CrossRef]
26. Zhang, P.; Yuan, G.F.; Shao, M.A.; Yi, X.B.; Du, T. Performance of the White method for estimating groundwater evapotranspiration under conditions of deep and fluctuating groundwater. *Hydrol. Process.* **2016**, *30*, 106–118. [CrossRef]
27. Wang, P.; Pozdniakov, S.P. A statistical approach to estimating evapotranspiration from diurnal groundwater level fluctuations. *Water Resour. Res.* **2014**, *50*, 2276–2292. [CrossRef]

28. Liu, Z.; Chen, H.; Huo, Z.; Wang, F.; Shock, C.C. Analysis of the contribution of groundwater to evapotranspiration in an arid irrigation district with shallow water table. *Agric. Water Manag.* **2016**, *171*, 131–141. [CrossRef]
29. Zhao, T.X.; Zhu, Y.; Ye, M.; Yang, J.Z.; Jia, B.; Mao, W.; Wu, J.W. A new approach for estimating spatial-temporal phreatic evapotranspiration at a regional scale using NDVI and water table depth measurements. *Agric. Water Manag.* **2022**, *264*, 107500. [CrossRef]
30. Henn, B.; Painter, T.H.; Bormann, K.J.; McGurk, B.; Flint, A.L.; Flint, L.E.; White, V.; Lundquist, J.D. High-elevation evapotranspiration estimates during drought: Using streamflow and NASA Airborne Snow Observatory SWE Observations to Close the Upper Tuolumne River Basin Water Balance. *Water Resour. Res.* **2018**, *54*, 746–766. [CrossRef]
31. Oki, T.; Kanae, S. Global hydrological cycles and world water resources. *Science* **2006**, *313*, 1068–1072. [CrossRef]
32. Trenberth, K.E.; Smith, L.; Qian, T.T.; Dai, A.G.; Fasullo, J. Estimates of the global water budget and its annual cycle using observational and model data. *J. Hydrometeorol.* **2007**, *8*, 758–769. [CrossRef]
33. Yeh, P.J.F.; Famiglietti, J.S. Regional groundwater evapotranspiration in illinois. *J. Hydrometeorol.* **2009**, *10*, 464–478. [CrossRef]
34. Cohen, D.; Person, M.; Daannen, R.; Locke, S.; Dahlstrom, D.; Zabielski, V.; Winter, T.C.; Rosenberry, D.O.; Wright, H.; Ito, E.; et al. Groundwater-supported evapotranspiration within glaciated watersheds under conditions of climate change. *J. Hydrol.* **2006**, *320*, 484–500. [CrossRef]
35. Xu, X.; Sun, C.; Qu, Z.; Huang, Q.; Ramos, T.; Huang, G. Groundwater recharge and capillary rise in irrigated areas of the upper Yellow River basin assessed by an agro-hydrological model. *Irrig. Drain.* **2015**, *64*, 587–599. [CrossRef]
36. Ayars, J.E.; Schoneman, R.A. Use of saline water from a shallow water table by cotton. *Trans. ASAE* **1986**, *29*, 1674–1678. [CrossRef]
37. Soppe, R.W.O.; Ayars, J.E. Characterizing groundwater use by safflower using lysimeters. *Agric. Water Manag.* **2003**, *60*, 59–71. [CrossRef]
38. Chen, Y.F.; Zhang, L.W.; Shi, W.; Ban, Y.; Liu, H.L.; Zhang, D.Y. Life history responses of spring-and autumn-germinated ephemeral plants to increased nitrogen and precipitation in the Gurbantunggut Desert. *Sci. Total Environ.* **2019**, *659*, 756–763. [CrossRef]
39. Yue, W.; Wang, T.; Franz, T.E.; Chen, X. Spatiotemporal patterns of water table fluctuations and evapotranspiration induced by riparian vegetation in a semiarid area. *Water Resour. Res.* **2016**, *52*, 1948–1960. [CrossRef]
40. Liu, H.; Yu, Y.; Zhao, W.; Guo, L.; Liu, J.; Yang, Q. Inferring subsurface preferential flow features from a wavelet analysis of hydrological signals in the Shale Hills Catchment. *Water Resour. Res.* **2020**, *56*, e2019WR026668. [CrossRef]
41. Martinez-de la Torre, A.; Miguez-Macho, G. Groundwater influence on soil moisture memory and land-atmosphere fluxes in the Iberian Peninsula. *Hydrol. Earth Syst. Sci.* **2019**, *23*, 4909–4932. [CrossRef]
42. Doorenbos, J.; Pruitt, W. *Guidelines for Predicting Crop Water Requirements*; UNFAO: Rome, Italy, 1975.
43. Holmes, J.W. Measuring evapotranspiration by hydrological methods. *Agric. Water Manag.* **1984**, *13*, 29–40. [CrossRef]
44. Tilahun, K.; John, L. Evapotranspiration estimation using soil water balance, weather and crop data. In *Evapotranspiration—Remote Sensing and Modeling*; IntechOpen: Rijeka, Croatia, 2012; pp. 41–57. [CrossRef]
45. Yi, L.H. Estimation of Groundwater Recharge Using Multiple Approaches: A Case Study in the Ordos Plateau. Master's thesis, University of Geosciences, Beijing, China, 2011. (In Chinese)
46. White, W.A. *Method of Estimating Ground-Water Supplies Based on Discharge by Plants and Evaporation from Soil: Results of Investigations in Escalante Valley, Utah*; Water Supply; U.S. Government Printing Office: Washington, DC, USA, 1932. [CrossRef]
47. Li, Z.; Liu, H.; Zhao, W.; Yang, Q.; Yang, R.; Liu, J. Quantification of soil water balance components based on continuous soil moisture measurement and Richards equation in an irrigated agricultural field of a desert oasis. *Hydrol. Earth Syst. Sci.* **2019**, *23*, 4685–4706. [CrossRef]
48. Allen, R.G.; Pereira, L.S.; Raes, D. *Crop Evapotranspiration: Guidelines for Computing Crop Water Requirements*; FAO Irrigation and Drainage Paper 56; FAO: Rome, Italy, 1998.
49. Healy, R.W.; Cook, P.G. Using groundwater levels to estimate recharge. *Hydrogeol. J.* **2002**, *10*, 91–109. [CrossRef]
50. Li, X.; Jin, M.; Zhou, N.; Huang, J.; Jiang, S.; Telesphore, H. Evaluation of evapotranspiration and deep percolation under mulched drip irrigation in an oasis of Tarim basin, China. *J. Hydrol.* **2016**, *538*, 677–688. [CrossRef]
51. Jorenush, M.H.; Sepaskhah, A.R. Modelling capillary rise and soil salinity for shallow saline water table under irrigated and nonirrigated conditions. *Agric. Water Manag.* **2003**, *61*, 125–141. [CrossRef]
52. Van Genuchten, M.T. A closed-form equation for predicting the hydraulic conductivity of unsaturated soils. *Soil Sci. Soc. Am. J.* **1980**, *44*, 892–898. [CrossRef]
53. Crosbie, R.S.; Binning, P.; Kalma, J.D. A time series approach to inferring groundwater recharge using the water table fluctuation method. *Water Resour. Res.* **2005**, *41*, W01008. [CrossRef]
54. Perez, P.J.; Castellvi, F.; Ibanez, M.; Rosell, J.I. Assessment of reliability of Bowen ratio method for partitioning fluxes. *Agric. Forest Meteorol.* **1999**, *97*, 141–150. [CrossRef]
55. Zou, T.; Li, Y.; Xu, H.; Xu, G.Q. Responses to precipitation treatment for *Haloxylon ammodendron* growing on contrasting textured soils. *Ecol. Res.* **2010**, *25*, 185–194. [CrossRef]
56. Guo, X.Y.; Feng, Q.; Si, J.H.; Xi, H.Y.; Zhao, Y.; Deo, R.C. Partitioning groundwater recharge sources in multiple aquifers system within a desert oasis environment: Implications for water resources management in endorheic basins. *J. Hydrol.* **2019**, *579*, 124212. [CrossRef]

57. Wang, W.H.; Chen, Y.N.; Wang, W.R.; Zhu, C.G.; Chen, Y.P.; Liu, X.G.; Zhang, T.J. Assessing and delineation of groundwater recharge areas in coastal arid area southern Tunisia. *J. Hydrol.* **2023**, *18*, 128936. [CrossRef]
58. Foken, T. The energy balance closure problem: An overview. *Ecol. Soc. Am.* **2008**, *18*, 1351–1367. [CrossRef]
59. Gao, X.; Mei, X.; Gu, F.; Hao, W.; Gong, D.; Li, H. Evapotranspiration partitioning and energy budget in a rainfed spring maize field on the Loess Plateau. China. *Catena* **2018**, *166*, 249–259. [CrossRef]
60. Yin, L.; Hu, G.; Huang, J.; Wen, D.; Dong, J.; Wang, X.; Li, H. Groundwater recharge estimation in the Ordos Plateau, China: Comparison of methods. *Hydrogeol. J.* **2011**, *19*, 1563–1575. [CrossRef]